




# Investigation of morphology and dielectric properties of PVDF composite films reinforced with MWCNT@PDA core–shell nanorods

Yating Yu<sup>1</sup>, Hang Xu<sup>1</sup>, Xiaoming Wang<sup>1</sup>, Lizhu Guan<sup>1</sup>, Xiaorui Zhang<sup>1,2</sup>, Zijian Wu<sup>1,2</sup>, and Ling Weng<sup>1,2,\*</sup> 

<sup>1</sup>School of Materials Science and Chemical Engineering, Harbin University of Science and Technology, Harbin 150040, China

<sup>2</sup>Key Laboratory of Engineering Dielectric and Its Application, Harbin University of Science and Technology, Ministry of Education, Harbin 150080, China

Received: 17 August 2021

Accepted: 27 January 2022

Published online:

15 February 2022

© The Author(s), under exclusive licence to Springer Science+Business Media, LLC, part of Springer Nature 2022

## ABSTRACT

This paper chooses to use polyvinylidene fluoride (PVDF) as the matrix, multi-walled carbon nanotubes (MWCNT) modified by polydopamine (PDA) as fillers, to prepare the MWCNT@PDA/PVDF composite films with excellent energy storage characteristics. The films were prepared by solution tape casting MWCNT@PDA/PVDF and MWCNT/PVDF composite films. The microstructures and properties of the composite films, especially the dielectric property, were investigated and the effect of MWCNT@PDA was analyzed. Results indicated that with the increase of filler content, the dispersion effect of filler in matrix becomes worse, and the energy storage modulus and dielectric constant increase gradually. When the content of MWCNT@PDA is 2.0 wt%, the dielectric constant of the MWCNT@PDA/PVDF composite film reaches 10.5 at 100 Hz, and the dielectric loss is 0.023. The addition of MWCNT@PDA is beneficial to increase the energy storage density of the composite membrane. When the content of MWCNT@PDA is 1.5 wt%, the energy storage density is 0.62 J/cm<sup>3</sup>, which is 2.7 times that of the pure membrane.

## 1 Introduction

As one of the three major electrical energy storage devices, dielectric containers have the advantages of high-power density, fast charging and discharging, wide operating temperature range, long cycle time, and low environmental pollution, etc. [1]. With the rapid development of electronic equipment, the

applications of dielectric containers in dielectric materials, power electronics, and other fields become more extensive [2]. In recent years, the integration and miniaturization of components in electrical appliances require dielectric materials with higher dielectric constant, lower dielectric loss, high breakdown field strength, and good mechanical properties [3–8]. Therefore, the development of complementary

Address correspondence to E-mail: wengling79@163.com

advantages of multiphase composites is particularly critical.

Polyvinylidene fluoride (PVDF) is inexpensive with high sensitivity, low dielectric constant, low dielectric loss, and high breakdown field strength, etc., so that PVDF is the most widely studied polymer dielectric material at present. Ceramic powders are used as dielectric fillers to improve the dielectric properties of composites because of their high dielectric constant [9–12]. Huang et al. prepared polymer functional composites by solution casting method with polyvinylidene fluoride (PVDF) as matrix and  $(\text{Ba}_{0.5}\text{Sr}_{0.4}\text{Ca}_{0.1})\text{TiO}_3$  (BSCT) as filler. The dielectric constant of BSCT/PVDF composites is 132 at 100 Hz and the dielectric loss is 0.005 at 1 GHz [13]. Lu et al. studied the effect of BCZT particles on the characteristics of composite films by solution casting method with doped  $47(\text{Ba}_{0.7}\text{Ca}_{0.3})\text{TiO}_3-0.53\text{Ba}(\text{Zr}_{0.2}\text{Ti}_{0.8})\text{O}_3$  into polyvinylidene fluoride, and the energy storage density reached the maximum value of  $3.69\text{ J/cm}^3$  when the content of BCZT was 20 vol% [14].

Comparing with ceramic-filled dielectric polymer composites, the conductive filler-filled type can achieve a high dielectric constant at lower filling content, which is expected to improve the energy storage density greatly while maintaining the good processing properties of the polymer. Wang et al. prepared multiwalled carbon nanotubes (MWCNTs) nested polyvinylidene fluoride (PVDF) microfibers using electrospinning technology and formed a stable three-dimensional conductive network when the content of CNTs was 1.2 wt% [15]. Zhao prepared the PVDF/CNT composite, and the dielectric loss was 3.51 when the dielectric constant was 80.6 [16]. He found the combination of carbon nanotubes (CNT) and graphene (GE) was chosen as inorganic fillers to form synergetic modification of poly(phenylene oxide) (PPO). PPO-based composite with 1.0 wt% GE and 7.5 wt% CNT exhibited dielectric permittivity of 283 at 1 kHz [17]. Eshraghian incorporation of 0.5 wt% nanoclay into N-CNT/PVDF nanocomposite at 1.0 wt% N-CNT loading resulted in 61% reduction in the dissipation factor [18]. Wannara prepared the NBR/BT-CNT composite with 80 phr BT and 1–2 phr CNT had dielectric constant of 100–500 [19]. Wang reported that a frontal ring-opening metathesis polymerization was used to in situ prepare polydicyclopentadiene (PDCPD)/carbon nanotubes (CNTs) and PDCPD/CNT-NH<sub>2</sub> composite. The PDCPD/CNT-NH<sub>2</sub>

composites exhibited high dielectric permittivity (47.5 at a frequency of 100 Hz) [20]. Liang successfully optimized the compact structure of a chlorine-doped continuous CNT sheet/polyvinylidene fluoride (Cl-CNT sheet/PVDF) by means of a hot-press treatment. The dielectric permittivity was 40.4 and the dielectric loss was 0.16 at  $10^2$  Hz [21]. Silakaew prepared the CNT-BT/PVDF composite. At  $10^3$  Hz, the low tan delta and sigma values of the CNT-BT/PVDF composite are about 0.06 and  $6.82 \times 10^{-9}\text{ S/cm}$  [22]. Deng prepared a kind of composite with V<sub>2</sub>C MXene-CNT hybrid particles as filler and environmentally friendly polyvinylalcohol (PVA) as matrix. The dielectric constant of 5 wt% ternary composite is close to 232, which is 122 times that of PVA [23]. In order to produce high energy storage materials with high dielectric constant and low dielectric loss, the new strategy of covering inorganic particles with an insulating layer to form a core-shell structure is a good choice [24]. Zhu reported that when 0.1 wt% 0.03PDA@CNTs were replaced by 0.2 wt% 0.2PDA@CNTs, the permittivity at  $10^3$  Hz was increased from 154 to 315 and the loss factor was reduced from 0.92 to 0.35 [25]. Cao found that insulating PVDF/SiC@PDA-a-30 composite containing 30 wt% of SiC@PDA-a had a dielectric constant of 35.1 while the dielectric loss still maintained as low as 0.037 at 1 kHz [26]. Feng found that 1.0 vol% PDA-SiO<sub>2</sub>@BT NFs/PVDF exhibited a high energy storage density of  $14.7\text{ J/cm}^3$  with an efficiency of 68% [27]. Guan et al. report the energy storage density of Ag@PDA/PVDF composites was 79.53% higher than that of pure PVDF films when the filler content was 10 wt% [28]. According to the references listed above, we can know that as a coating material with high surface activity, polydopamine can form an insulating barrier on the surface of conductive particles, binding the macroscopic movement of free carriers, reducing the dielectric loss, and has good compatibility with the polymer as a whole, which is beneficial to improve the comprehensive dielectric properties. This modification method shows a great advantage, but there are not too much researches on the effect of PDA modification of CNT on the dielectric properties of polymers.

In this paper, MWCNT@PDA nanorods with typical core-shell structure were obtained by the oxidation polymerization method of dopamine. A series of MWCNT@PDA/PVDF composites were prepared by doping different content of nano-sized nanorods into PVDF matrix. The microstructure, mechanical properties, and dielectric properties of the composite were

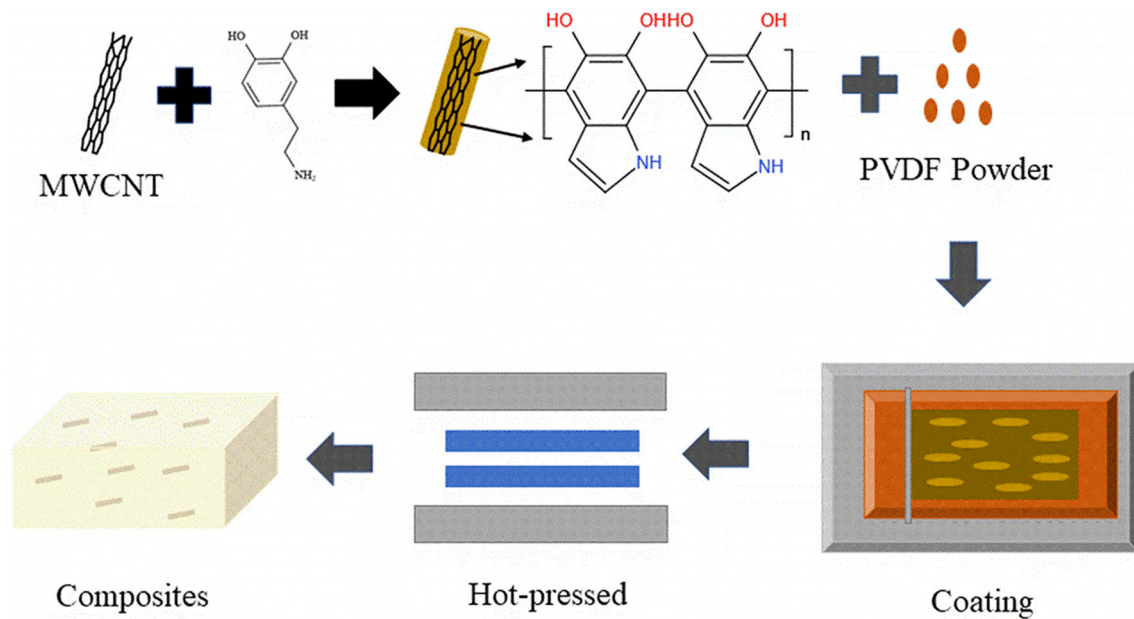


**Fig. 1** Preparation process of PVDF nanocomposite films

studied. The effect of MWCNT@PDA nanorods with core-shell structure on the microstructure and properties of the composite were discussed by comparing with the properties of MWCNT/PVDF composite.

## 2 Experiments

### 2.1 Material

Multiwalled carbon nanotubes (MWCNTs, length: 15–30  $\mu\text{m}$ , bulk density: 0.06–0.09  $\text{g}/\text{cm}^3$ ) were prepared by Shenzhen Turing Evolution Technology Co. Ltd. Polyvinylidene fluoride (PVDF,  $M_v$ :30,000) was purchased by Shanghai PeiHong New Material Co., Ltd. N, N-dimethylformamide (DMF) was offered by Tianjin XingAn Chemical Co., Ltd.. Dopamine hydrochloride (DA-HCl, 98%) and trimethyl-amino-methane hydrochloride (Tris, 99%) were obtained from Macklin, China.

### 2.2 Experiment

#### 2.2.1 Preparation of core-shell structured MWCNT@PDA

The preparation progress is shown in Fig. 1. Firstly, the tris aqueous solution ( $\text{pH} > 9$ ) was prepared by

120 mg tris and 100 g deionized water, and hydrochloric acid solution (0.2 mol/L) was added dropwise into the solution after it was stirred for 10 min to prepare the tris-HCl buffer solution ( $\text{pH} = 8.5$ ). 100 mg MWCNT was added into the Tris-HCl solution and ultrasonic for 1 h and 180 mg DA-HCl was added for water bath at 50  $^\circ\text{C}$  degrees for 4 h, 6 h, and 8 h (named No. 1, 2, and 3). Then the suspensions were centrifuged and washed three times by deionized water and dried at 50  $^\circ\text{C}$  for 12 h. Then the MWCNT@PDA core-shell nanorods were successfully obtained.

#### 2.2.2 Preparation of PVDF nanocomposite film

As shown in Fig. 1, an appropriate amount of polyvinylidene fluoride (PVDF) powder was dissolved in N, N-dimethylformamide (DMF), and sonicate for 2 h, and then added MWCNT or MWCNT@PDA nanoparticles, sonicate for 4 h. The whole solution was poured on glass mold and coated by the coating machine after vacuum de-gassing process. The coated films were cured at 80  $^\circ\text{C}$  for 12 h. Then the initial films were heat pressed at 180  $^\circ\text{C}$ , 15 MPa for 15 min. and cooled down to prepare the MWCNT/PVDF and MWCNT@PDA/PVDF composite films.

### 2.3 Characterization

Transmission electron microscope (TEM, JEM-2100) was used to observe the encapsulation of polydopamine (PDA) on the surface of MWCNT; XPS (ESCALAB 250) was used to assist in the verification of the encapsulation of the core-shell material; scanning electron microscopy (SEM, Apreo C) was used to observe the surface morphology of the core-shell material; scanned samples were first embrittled in liquid nitrogen and then gold was sprayed on the cross section to observe the dispersion of the filler in the matrix. The X-ray diffraction (XRD) patterns were obtained from X'Pert PRO, operating at 40 kV and 40 mA. The broadband impedance analyzer ((GmbH Novocontrol Alpha-A) was used to test the dielectric properties (dielectric constant, dielectric loss, and conductivity) of composite materials. The sample was 30 mm in diameter and about 100  $\mu\text{m}$  thick, and a thin aluminum coating of 25 mm in diameter was applied to the front and back sides of the disk as electrodes. The DC breakdown strength was assessed by an LAS6030P electrical breakdown strength tester at room temperature with an increasing voltage rate of 800 V/s, which was supplied by Boher High Voltage Power Supplies Co. Ltd, China. A ferroelectric integrated measuring instrument (Precision Premier II) was used to test the ferroelectric polarization (D-E) behavior of the composite dielectric film. Before the test, it is necessary to vacuum-evaporate aluminum electrodes on the composite dielectric film samples, and the diameter of the holes in the upper and lower molds is about 3 mm.

## 3 Results and discussion

### 3.1 Microstructures of MWCNT@PDA core-shell material nanorods

The elemental analysis on carbon nanotube particles (MWCNT) which modified by polydopamine (PDA) was performed by XPS. The results are shown in Fig. 2. As can be seen from Fig. 2a, the ratio of C in MWCNT was decreased while the ratio of O was increased after modified by PDA, which means the oxygen-containing functional groups on modified MWCNT increased greatly. As a characteristic element of polydopamine, the increase of nitrogen showed that carbon nanotubes have been modified

by polydopamine successfully. It can be seen from Fig. 2b that the C atom in pure MWCNT exists as  $\text{sp}^2$  hybridization and  $\text{sp}^3$  hybridization mainly, so a strong peak appears at 284.8 eV. Similarly, CNT@PDA particles have an extra peak at 287.0 eV, and this peak is blue-shifted compared to the peak of pure polydopamine at 286.4 eV [29]. This is due to the reaction between polydopamine and carbon nanotubes. The C-O bond is more electronegative, and the fixing capacity of C atom nucleus to extranuclear electrons was increased, so the binding energy is improved, and the peak is shifted to high binding energy. As for the analysis of the N element, the peak of CNT@PDA at 402 eV [29] shifted to high binding energy, which should be attributed to the increase of electronegativity after the protonation of the N atom, As shown in Fig. 2c, d.

According to the different reacting time, the core-shell materials with different shell thickness can be obtained. As shown in Fig. 3, SEM a1-d1 shows that with the increase of coating time, the carbon tube outcrops increase. TEM, Fig. a2-d2, shows that with the increase of coating time, the thickness of CNTs first increases and then decreases, and the surface roughness of CNTs gradually increases. At the same time, high-resolution transmission electron microscopy (HRTEM) analysis showed that (a3-d3) the increase of coating time can effectively increase the thickness of PDA shell on CNT surface. However, if the coating time is too long, the self-polymerization of DA will increase, the amount of PDA adsorbed on the surface of CNT will decrease, and the thickness of PDA shell on the surface of CNT will become thinner. By comparing the smoothness and uniformity of the coating, it is concluded that the coating time of 6 h is the best.

### 3.2 XRD patterns of PVDF-based nanocomposite films

The crystalline state of the filler particles and the matrix have an important influence on the dielectric properties of the material. Figure 4 shows the XRD patterns of the sample with the testing angles from  $10^\circ$  to  $50^\circ$ . The results show that PVDF phase crystals appear in the figure, and the diffraction peak intensity of the composite material has changed compared with that of the pure film. The pure PVDF film has strong diffraction peaks at  $2\theta$  of  $17.6^\circ$ ,  $18.3^\circ$ ,  $19.93^\circ$ , and  $26.5^\circ$ , corresponding to the  $\alpha$  (100),  $\gamma$  (020),  $\gamma$

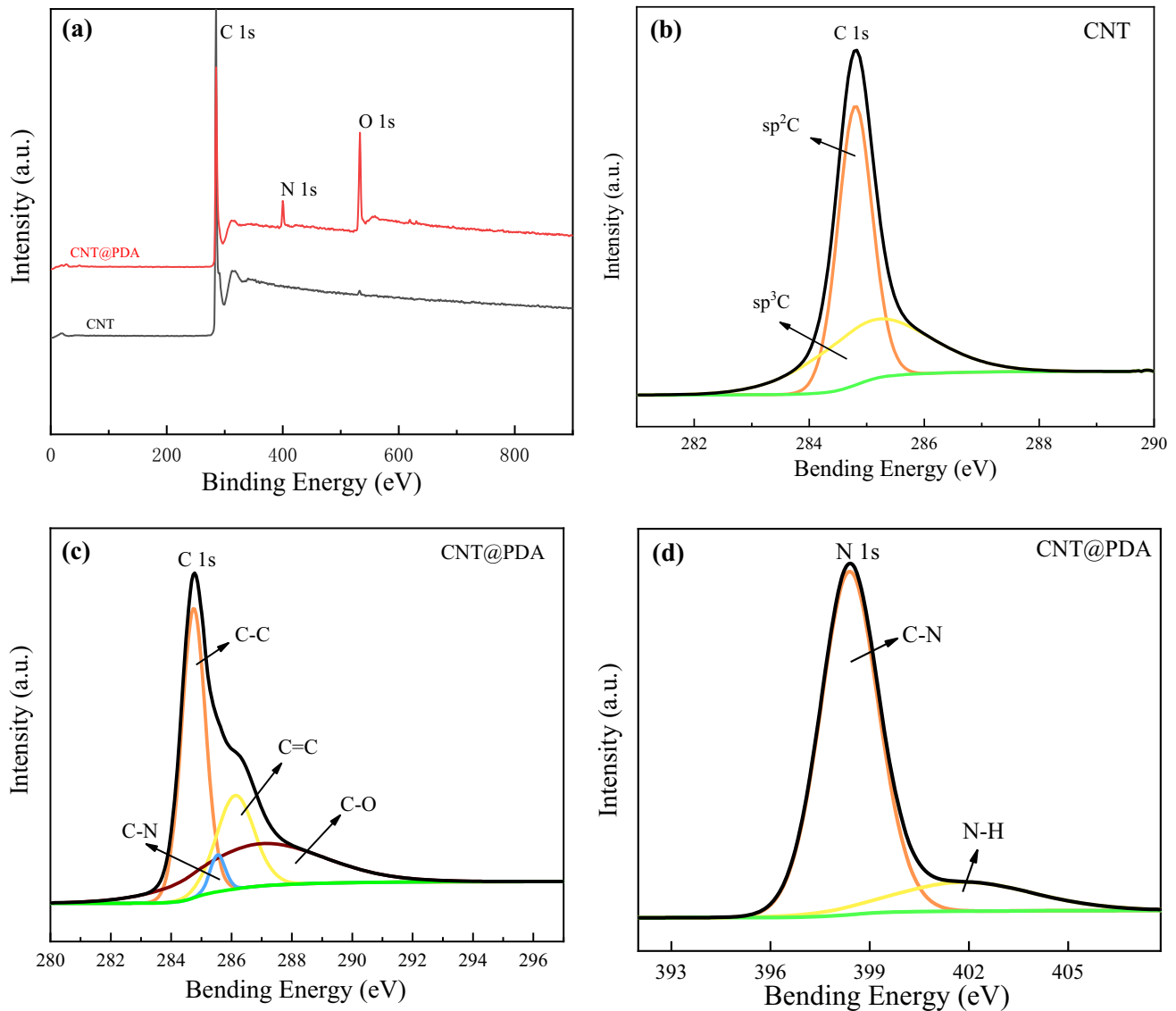


**Fig. 2** **a** XPS spectra of the MWCNT and MWCNT@PDA nanoplatelets, **b** C 1 s peaks at XPS spectra of MWCNT, **c**, **d** C 1 s and N1s peaks at XPS spectra of MWCNT@PDA nanoplatelets

(110), and  $\gamma$  (022) phases of PVDF crystals, respectively, which proves that there are more  $\alpha$  and  $\gamma$  phases in the PVDF film. It can be seen clearly that the addition of nano-filler made the diffraction peaks of  $\alpha$  (100),  $\gamma$  (020),  $\gamma$  (110), and  $\gamma$  (022) weaken. The MWCNT@PDA/PVDF and MWCNT@PDA/PVDF composite films showed diffraction peaks representing the  $\beta$  phase of the PVDF matrix at  $2\theta = 20.2^\circ$ . The changes in these diffraction peaks indicated that the PVDF shifts to a more polar crystalline phase after the fillers were added, which has an impact on the dielectric properties of PVDF-based composite films.

The three peaks located around  $18.5^\circ$ ,  $20.1^\circ$ , and  $26.6^\circ$   $2\theta$  are the (020), (110), and (022) diffractive crystal planes of the non-polar  $\gamma$  phase. The card number is 00–038–1638. The peak located near  $2\theta$  is about  $17.8^\circ$ , which is the (100) diffraction crystal plane of non-polar  $\alpha$ -phase PVDF, and the card number is 00–042–1650.

Figure 5 shows the SEM images of pure PVDF, MWCNT/PVDF, and MWCNT@PDA/PVDF membranes under different magnifications. It can be seen from the figure that the cross section of pure membrane is flat and there is almost no wrinkle on it.

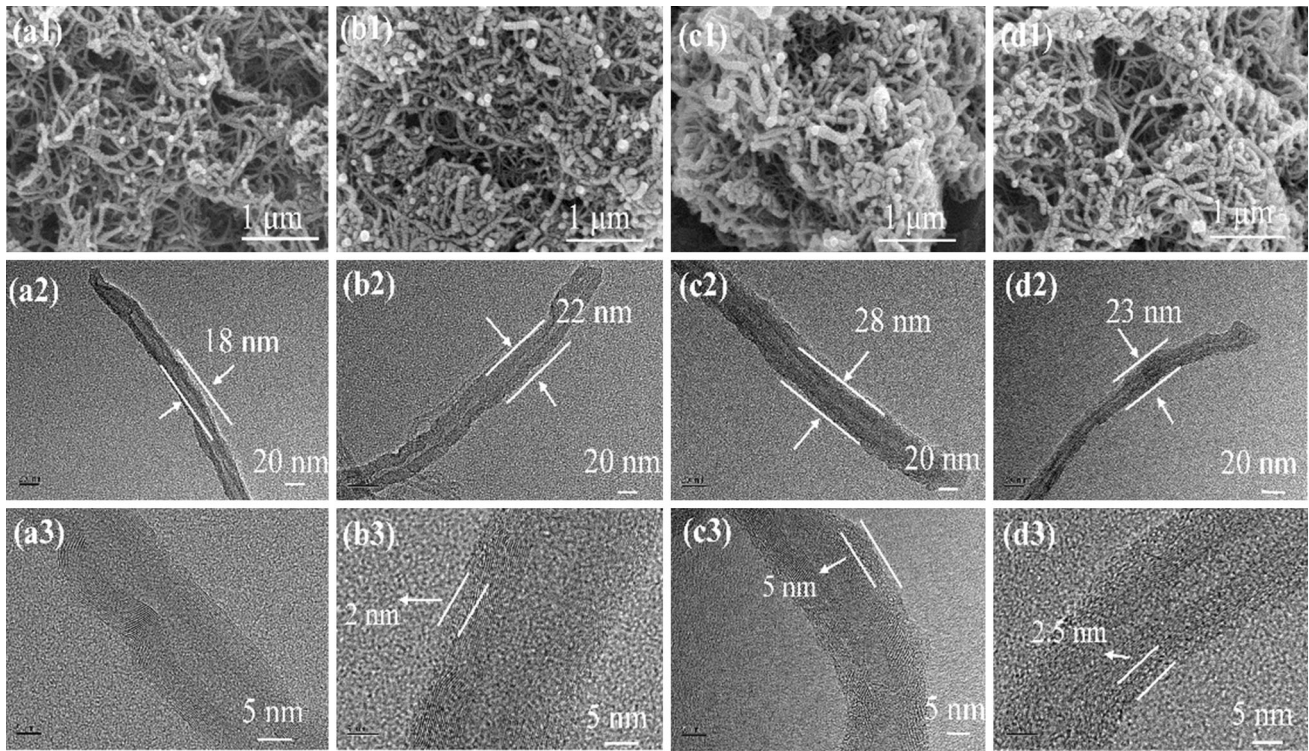


**Fig. 3** SEM micrographs (a1–d1) TEM micrographs (a2–d2) (a3–d3) of the coated time with 0 h, 4 h, 6 h, and 8 h

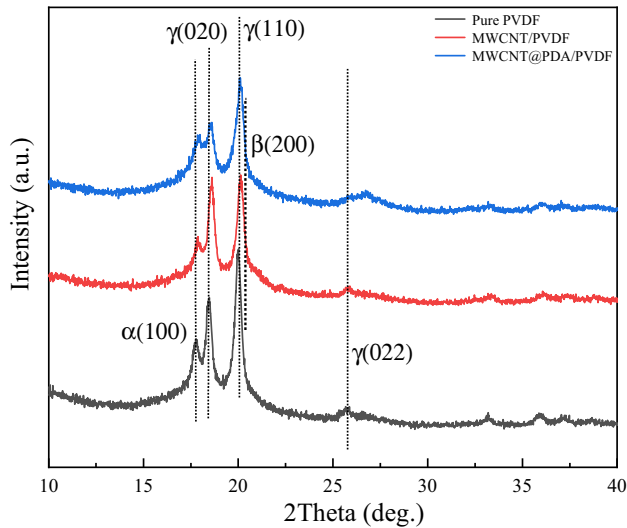


**Fig. 4** XRD diffractogram peak patterns of Pure PVDF, MWCNT/PVDF nanoplatelets, and MWCNT@PDA/PVDF nanoplatelets

Compared with the SEM image of the filler to be added, the distribution of the filler can be seen clearly, and the surface is uneven, especially when the filler content reaches 2.0 wt%, the carbon tubes are agglomerated. Compared with the

MWCNT@PDA/PVDF and MWCNT/PVDF, it can be seen that the MWCNT@PDA is distributed more evenly in the matrix, and no pores and cracks are observed between the two phases, which indicating that there is good compatibility between the filler and the matrix.

### 3.3 Dielectric properties of PVDF-based nanocomposite films

In order to verify the influence of the addition of fillers on the dielectric properties of the PVDF matrix, we tested the dielectric constant, dielectric loss, conductivity, and breakdown strength of the composite film. The test results are shown in Fig. 6 and Table 2. The dielectric constants of all composite films show a decreasing trend as the frequency increases. This is because the composite material will undergo dipole turning polarization when the frequency is  $10^3$ – $10^8$  Hz, and the dipoles in the composite film will turn around. Failure to keep up with the changes in the electric field at high frequencies shows that the dielectric constant decreases as the frequency increases, as shown in Fig. 6a, b. When the content of MWCNT was 2.0 wt%, the dielectric constant of

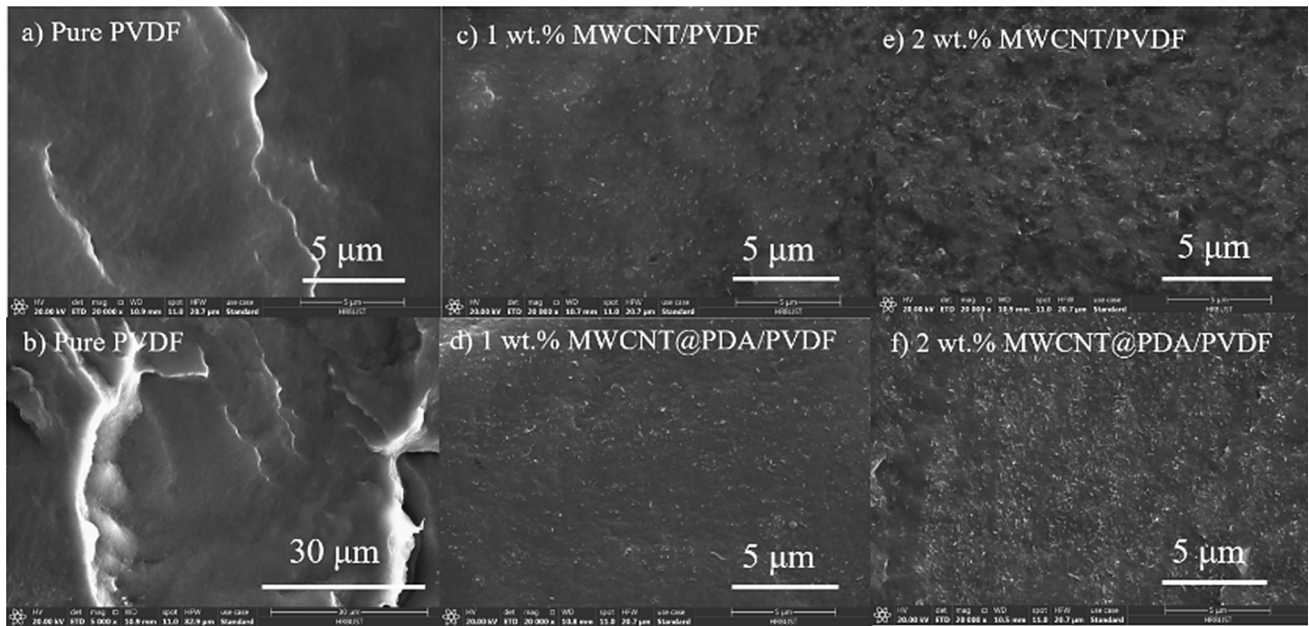


**Fig. 5** the brittle fracture cross-sectional morphology of the pure PVDF film and MWCNT@PDA/PVDF composite films with 1.0 wt% and 2.0 wt% MWCNT doping amount

MWCNT/PVDF composite films reached the maximum, which was about 5 times higher than that of pure PVDF. As shown in Fig. 6b, When the content of MWCNT@PDA is 2.0 wt%, the dielectric constant of MWCNT@PDA/PVDF composite films reaches the maximum value, as high as 10.5 at 100 Hz. Because MWCNTs are conductive, interface polarization occurs between MWCNTs and PVDF. Interface polarization has the greatest impact on MWCNT@PDA/PVDF composites, and the response time is the longest. With the increase of filler content, the number of phase interfaces increases, and the interfacial polarization effect also enhances, so the dielectric constant increases. It can be seen from Fig. 6a and b that the dielectric constant of MWCNT@PDA/PVDF decreases compared with MWCNT/PVDF when the amount of filler and frequency are the same. This is because the dielectric constant decreases with the increase of compatibility between the matrix and the filler. There are cavities between the unmodified MWCNT and the matrix. There are two interfaces which are MWCNT and cavities, cavities and PVDF. The compatibility of modified MWCNT with the matrix increases, and the number of cavities decrease. The filler is distributed more evenly in the matrix. After the electric field is applied, the space charge will accumulate at the

interface, and the dielectric constant of composites with more interfaces is much higher than that of composites with fewer interfaces.

The dielectric loss of the composite material depends on the dielectric loss of the matrix and the polarization degree of the interface between the matrix and the filler. When the filler was MWCNT and MWCNT@PDA, the relationship between dielectric loss and frequency is shown in Fig. 6c and d. As the frequency increases, the dielectric loss of the composite film first decreases and then increases. This is the relaxation characteristic of the dielectric material. At low frequencies, the dielectric loss is mainly caused by the polarization of the composite film's interface. It is caused by the relaxed polarization of the dipole. When the filler was MWCNT, the dielectric loss increases significantly with the increase of the filler content. Under the same frequency and the same filler content, the dielectric loss of the MWCNT@PDA/PVDF composite film decreases significantly. As the filler content increases, the dielectric loss will increase, but it is similar to the pure film phase. At 100 Hz, compared with these two fillers, the dielectric loss decreased by 85.1%, 88.1%, 89.6%, and 88.1% with the increase of filler content. It can be seen from Fig. 6c and d that dopamine coating is beneficial to reduce dielectric loss.

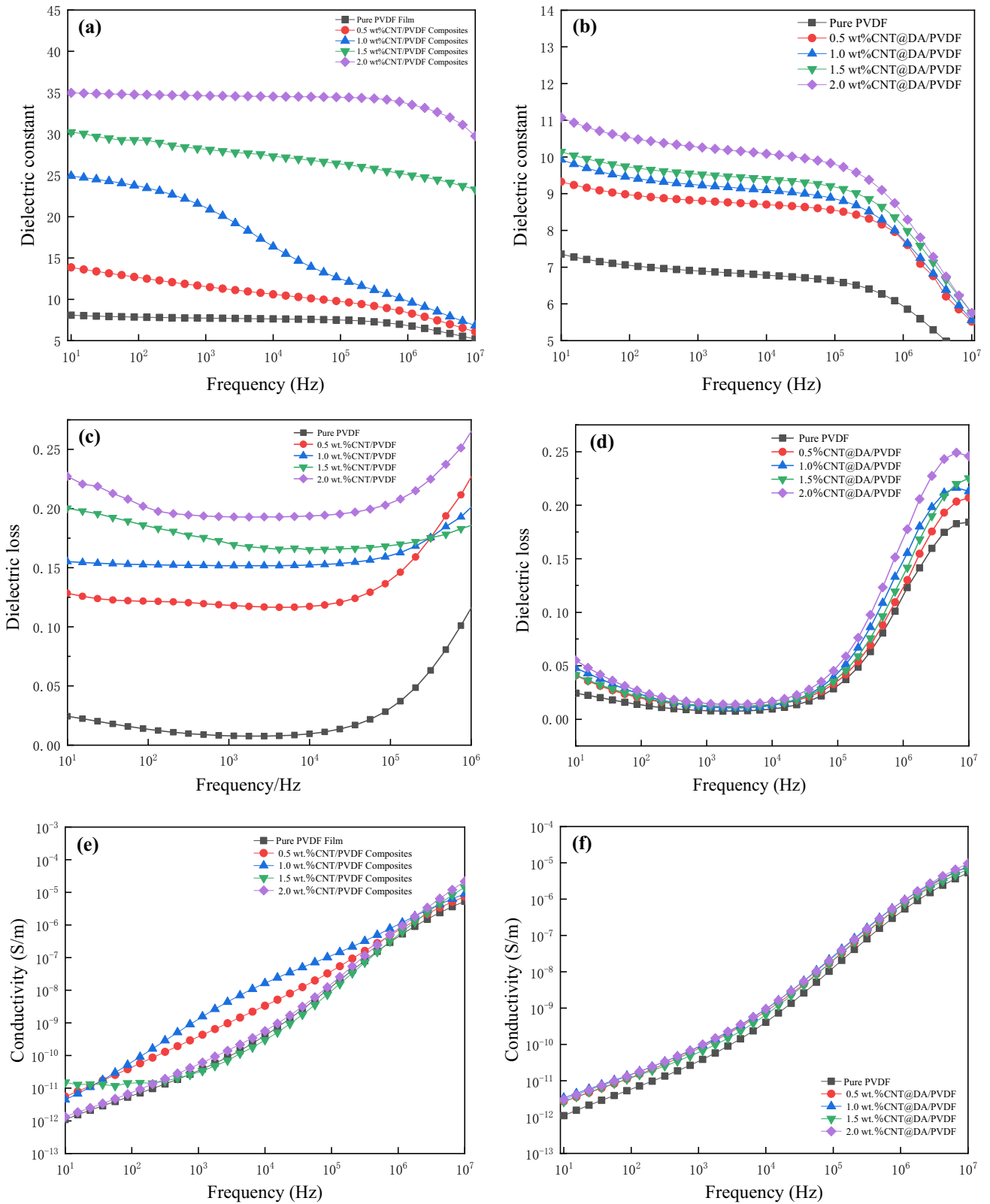


**Fig. 6** Dielectric constant, dielectric loss, and conductivity dependence of composite films as a function of frequency (a–f)



When CNT was added to the matrix PVDF, the conductivity of the composite film is significantly higher than that of the pure PVDF film. When CNT@PDA was added to the matrix PVDF, the conductivity increases with the increase of the filler addition, but it is lower than the CNT/PVDF composite film, as shown in Fig. 6e, f. Conductivity is an important parameter for evaluating the mobility of carriers in dielectric materials, which indicates that PDA has a certain ability to limit the mobility of carriers.

The breakdown strength of composite materials is another important factor for affecting the dielectric properties of dielectric materials. In order to reduce the experimental error, the two-parameter Weibull analysis method is used to process the breakdown strength data of composite materials. The main relationship is shown in formulas 1 and 2. It can be observed that after the filler was added, the breakdown strength began to decrease. With the increase of the filler content, the breakdown strength gradually decreases. According to the electron avalanche breakdown theory, space charge is one of the key factors affecting the breakdown field strength, and the more space charge is, the lower the breakdown field strength is, the addition of fillers makes a large number of nanocapacitors formed in the composite film, accumulating a large amount of space charges, and these space charges cause electric field distortion and reduce breakdown field strength.

$$P(E) = 1 - \exp\left(-\left(\frac{E}{E_0}\right)^\beta\right) \quad (1)$$

$$\ln(-\ln(1-p)) = \beta(\ln E - \ln E_0) \quad (2)$$

where  $P(E)$  represents the cumulative failure probability, and  $E$  and  $E_0$  are the test breakdown strength value and breakdown strength at  $P(E_0) = 63.28\%$ , respectively;  $\beta$  is the shape parameter. Equation 2 is obtained by logarithmic processing of both sides of Eq. 1 [30]. The results are shown in Fig. 7 and Table 1.

The dielectric properties and breakdown strength of this composite have been introduced above. We also studied the polarization behavior and ferroelectric properties (D-E curves) of the composites which were shown in Fig. 8. As the increasing of the filler content, the maximum electric field strength of the composite was gradually reduced. When the MWCNT@PDA content was 0 wt%, 0.5 wt%, 1.0 wt%, 1.5 wt%, and 2.0 wt%, the maximum electric displacement of the composites under 1800 kV/cm,

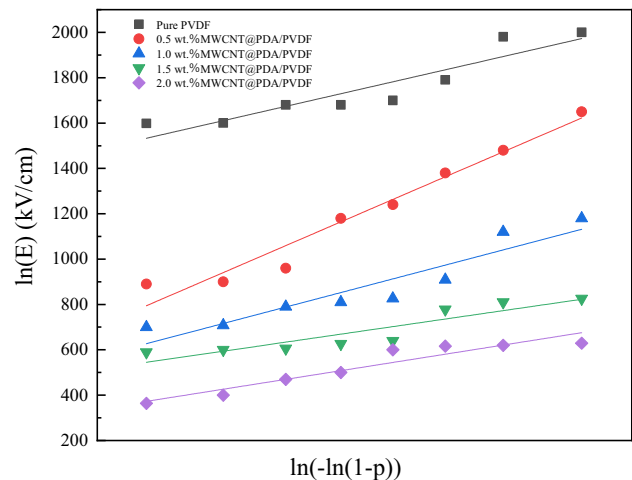


**Fig. 7** Weibull breakdown field strength image of MWCNT@PDA/PVDF film

**Table 1** The composite material of pure PVDF and different content of MWCNT@PDA filler

Sample	Weibull parameter	
	$\beta$	$E_B$ (kV/cm)
Pure PVDF	196.28	1824.95
0.5 wt% CNT@PDA/PVDF	369.67	1317.60
1.0 wt% CNT@PDA/PVDF	225.21	952.28
1.5 wt% CNT@PDA/PVDF	124.11	727.42
2.0 wt% CNT@PDA/PVDF	135.18	565.52

1100 kV/cm, 900 kV/cm, 700 kV/cm, and 600 kV/cm electric fields was about  $3.20 \mu\text{C}/\text{cm}^2$ ,  $3.58 \mu\text{C}/\text{cm}^2$ ,  $3.16 \mu\text{C}/\text{cm}^2$ ,  $3.24 \mu\text{C}/\text{cm}^2$ , and  $1.77 \mu\text{C}/\text{cm}^2$ . This increase in the electric displacement of the composite medium is mainly due to the high dielectric constant of MWCNT@PDA. As the content of the filling phase increased, more bounded electric charge appeared between the interfaces, the number of defects in the composite increased, and the maximum electric field strength of MWCNT@PDA/PVDF gradually decreased. As the Fig. 8 shown, when the MWCNT@PDA was low, The D-E curve of the composite showed as a saturation trend. It is not conducive for the enhancement of the energy storage density and efficiency if the saturation trend appeared too early when the composite was affected by a high electric field or a low electric displacement. As the increasing of the contents, the energy storage density and efficiency of the composite are developing due to the delayed saturation trend of the composite.

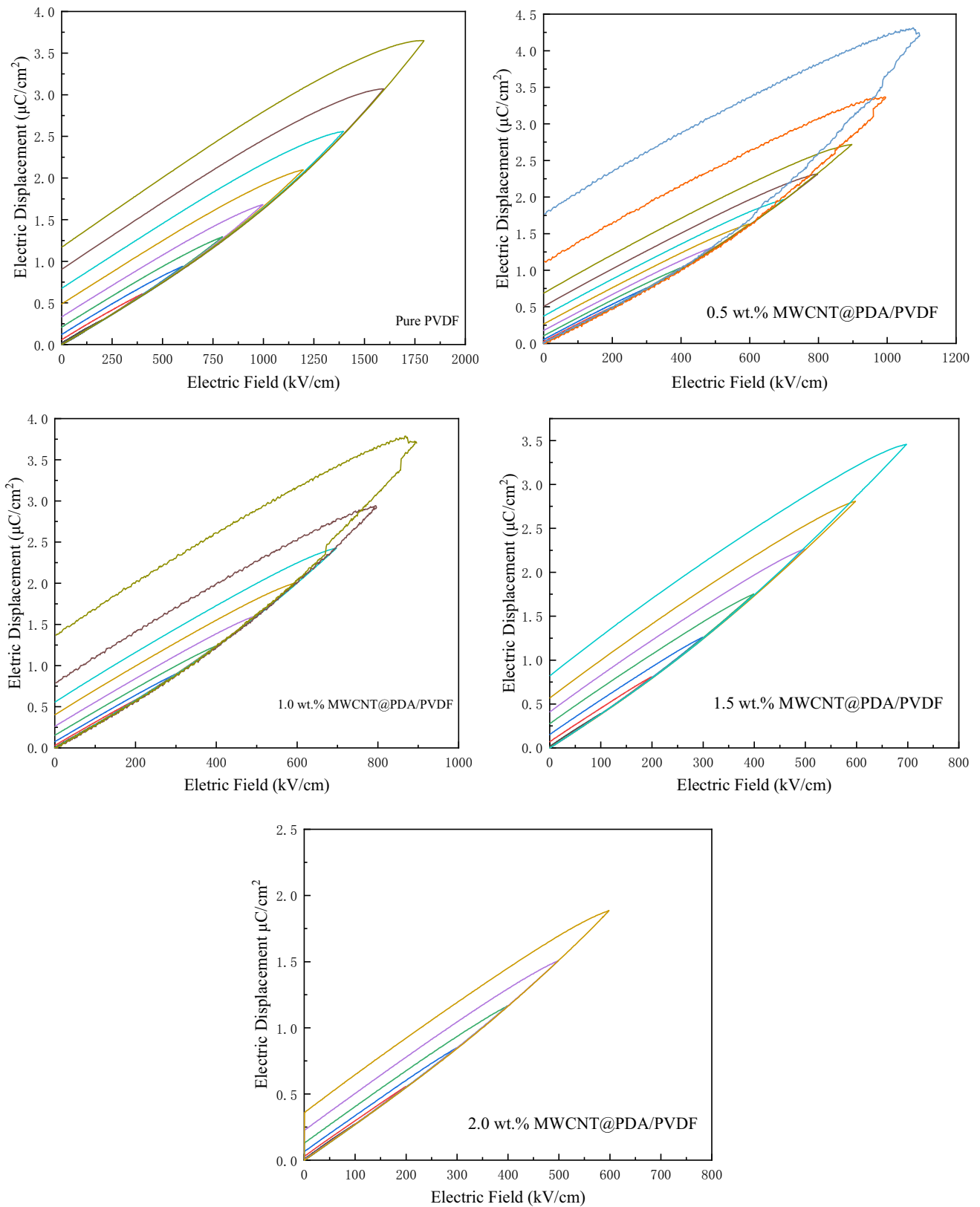


**Fig. 8** The D-E graph of x wt% MWCNT@PDA/PVDF

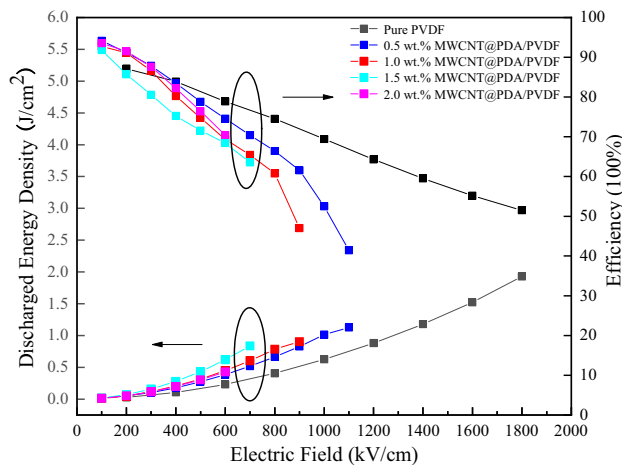


**Fig. 9** Energy storage performance-electric field curve of PVDF matrix composite medium

The final energy storage results are obtained by calculating through Eq. (3), (4) and the D-E curve of the composite is shown in Fig. 9 and Table 2.

$$\eta = \frac{U_e}{\int_0^{D_m} E dD} \quad (3)$$

$$\chi_C = \frac{\Delta H_m}{\Delta H_{100}} \times 100\% \quad (4)$$

When the MWCNT@PDA contents were 0 wt%, 0.5 wt%, 1.0 wt%, 1.5 wt%, and 2.0 wt%, the discharge energy density of PVDF matrix composites was about 0.23 J/cm<sup>3</sup>, 0.38 J/cm<sup>3</sup>, 0.45 J/cm<sup>3</sup>, 0.62 J/cm<sup>3</sup>, and 0.43 J/cm<sup>3</sup> at the same electric field strength of 600 kV/cm, and the discharge efficiency at this energy storage density was 78.87%, 74.55%, 69.34%, 68.40%, and 70.43%, respectively. The addition of MWCNT@PDA was benefit to improve the energy storage density of the composite film, which was 2.7 times higher than that of the pure film when the filler content was 1.5 wt.%. It can be seen from the data

**Table 2** Dielectric constant, dielectric loss of different composite at 100 Hz, energy storage of different composite at 600 kV/cm

Sample	Dielectric constant	Dielectric loss	Energy storage (600 kV/cm)
Pure PVDF	7.85	0.013	0.231
0.5 wt% CNT/PVDF	12.71	0.121	–
1.0 wt% CNT/PVDF	23.77	0.152	–
1.5 wt% CNT/PVDF	29.25	0.186	–
2.0 wt% CNT/PVDF	34.77	0.201	–
0.5 wt% CNT@PDA/PVDF	8.98	0.020	0.384
1.0 wt% CNT@PDA/PVDF	9.46	0.024	0.447
1.5 wt% CNT@PDA/PVDF	9.74	0.021	0.619
2.0 wt% CNT@PDA/PVDF	10.54	0.026	0.426

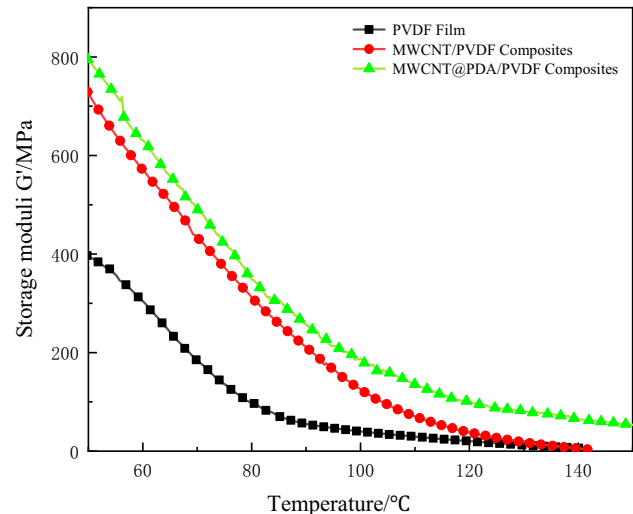


**Fig. 10** Dynamic mechanical analysis of PVDF film and its composites with MWCNT and MWCNT@PDA nanorods addition at 1.5 wt% content

that the energy storage density of the composite increased first and then decreased as the MWCNT@PDA contents increasing. When the content was appropriate, the energy storage density reached maximum value. As the electric field increased, the energy storage efficiency decreased gradually, which may be due to the presence of defects in the composite, which led to high energy loss in the material. When the MWCNT@PDA content was 1.5 wt.%, the energy storage density of the composite was higher, and the efficiency can reach 68.40% still, which is attributed to the reduced dielectric loss of the composite after the surface modified by polydopamine, which reduced the internal defects of the composite film.

**Fig. 11** Finite element simulation of electric field strength for two kinds of composites

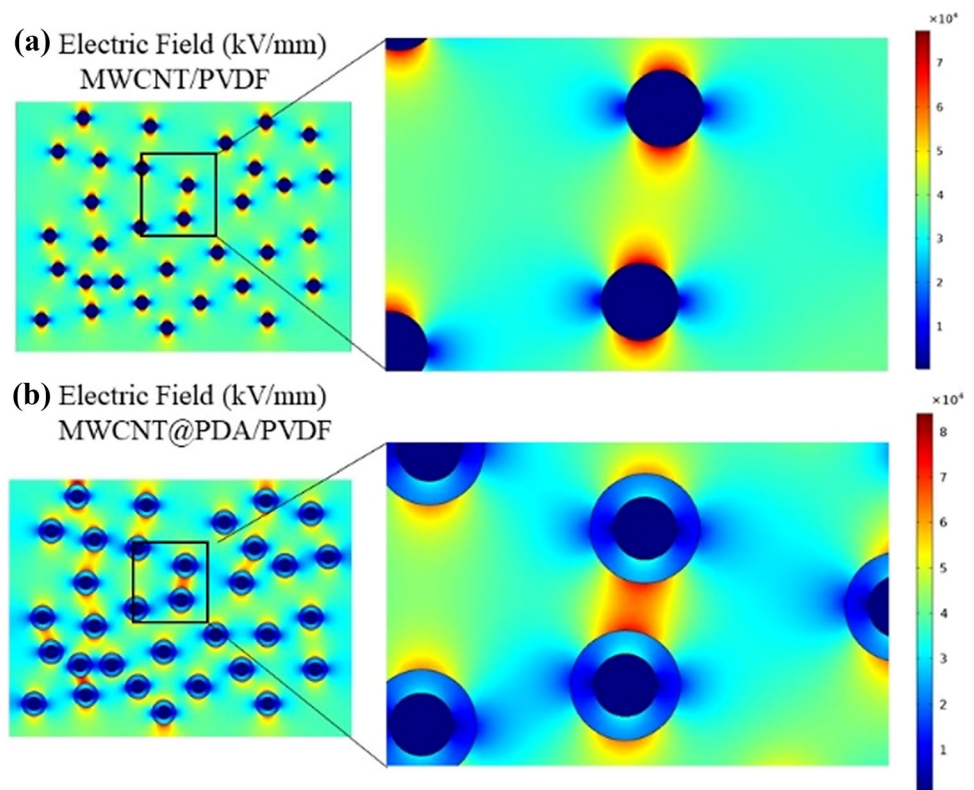


Figure 10 shows the dynamic mechanical analysis of PVDF film and its composites with MWCNT and MWCNT@PDA nanorods at 1.5 wt% content from the temperature of 50–140 °C. As can be seen from the figure, the initial energy storage modulus of the composites increased significantly with the doping of MWCNT and MWCNT@PDA, and the MWCNT@PDA/PVDF composite film was slightly higher than the MWCNT/PVDF composite film at the same temperature. The steady increasing of the energy storage modulus was attributed to the mechanical occlusion between the MWCNT@PDA and the PVDF matrix, which effectively facilitated the force transfer between the filler and the matrix. Further analysis leads to the conclusion that the filler type also has an effect on the energy storage modulus of the composite films. The energy storage modulus of MWCNT@PDA/PVDF composite films and MWCNT/PVDF composite films at 50 °C was 729 MPa and 710 MPa, which were 1.84 and 1.79 times higher than those of pure PVDF. This is due to the fact that in the MWCNT@PDA/PVDF composite system, the addition of MWCNT@PDA nanorods made the alignment of the PVDF matrix chain segments in a more regular direction, and the polarity of

the  $\beta$ -phase of PVDF is usually higher than that of the  $\alpha$  and  $\gamma$ -phases in PVDF, during the continuous movement of the molecular chain forging, the polar groups can increase the frictional resistance between the molecular chain forging, resulting in a stronger interaction, which improved the storage modulus of the composite film eventually, and this change is consistent with the XRD results.

Based on the analysis of the experimental results above, finite element simulations of PVDF composites with different fillers were carried out by COMSOL Multiphysics to demonstrate the distribution of electric field intensity inside the composites, which is shown in Fig. 11. In MWCNT@PDA/PVDF composite films, the interaction between the particles was enhanced, but the dopamine shell reduced the extent of electric field distortion and the red electric field strength region around the particles was reduced, as shown in Fig. 11b. Therefore, the simulated structure also confirmed further that the dopamine shell around MWCNT was beneficial to enhance the breakdown field strength of the composite film.

## 4 Conclusion

In conclusion, we synthesized a new MWCNT@PDA nanorods successfully, and the microstructure of MWCNT@PDA was analyzed by SEM, TEM, XPS, and other means, which confirmed that a new core-shell structure was synthesized, and this kind of nanorods were used to improve the dielectric properties of PVDF, and MWCNT@PDA and single MWCNT were compounded with PVDF to prepare composite films, and a series tests results showed that MWCNT@PDA/PVDF has a better dielectric properties and breakdown field strength. The results indicated that MWCNT@PDA nanorods can induce the phase transition from  $\alpha$  to  $\beta$  and  $\gamma$  of PVDF composite more effectively; in another words, the core shell structure led to a significant enhancement of the polarization of the PVDF matrix, which indicated that the MWCNT@PDA/PVDF composites has better electrical properties.

## Acknowledgements

The authors are thankful for the financial supports from the National Natural Science Foundation of China (51677045, 51177030), the Natural Science Foundation of Heilongjiang Province (E201224), and Harbin Science and Technology Innovation Talent program (2016RAQXJ059).

## Author Contributions

YY and HX of this article contributed the same. YY performed experimental design and writing-review and editing. HX involved in analysis of experimental data. XW participated in data curation. LG and ZW involved in investigation. XZ provided the experimental analysis suggestion. LW performed resources and supervision.

## Declarations

**Conflict of interest** The authors declare that there is no conflict of interests regarding the publication of this paper.

**Data Availability** The data that support the findings of this study are available from the corresponding author upon reasonable request.

## References

1. X.H. Hao, J. Adv. Dielectr. **3**, 1330001 (2013)
2. T. Kousksou, P. Bruel, A. Jamil, T. El Rhafiki, Y. Zeraouli, Sol. Energy Mater. Sol. Cells **120**, 59–80 (2014)
3. B.J. Chu, X.Z. Zhou, K.L. Ren, B. Neese, M.R. Lin, Q. Wang, F. Bauer, Q.M. Zhang, Science **313**, 334–336 (2006)
4. P.W. Zhu, L. Weng, X.R. Zhang, X.M. Wang, L.Z. Guan, L.Z. Liu, J. Mater. Sci. **55**, 7665–7679 (2020)
5. A. Azizi, M.R. Gadinski, Q. Li, M.A. AlSaud, J. Wang, Y. Wang, B. Wang, F.H. Liu, L.Q. Chen, N. Alem, Q. Wang, Adv Mater **29**, 1701864 (2017)
6. Y. Yang, H.L. Sun, D. Yin, Z.H. Lu, J.H. Wei, R. Xiong, J. Shi, Z.Y. Wang, Z.Y. Liu, Q.Q. Lei, Journal of Materials Chemistry A **3**, 4916–4921 (2015)
7. Q. Wang, L. Zhu, J. Polym. Sci., Part B: Polym. Phys. **49**, 1421–1429 (2011)
8. Z. Wang, T. Wang, M.R. Fang, C. Wang, Y.J. Xiao, Y.P. Pu, Compos. Sci. Technol. **146**, 139–146 (2017)
9. K.C. Li, H. Wang, F. Xiang, W.H. Liu, H.B. Yang, Appl. Phys. Lett. **95**, 202904 (2009)
10. J.J. Li, J. Claude, L.E. Norena-Franco, S.I. Seok, Q. Wang, Chem. Mater. **20**, 6304–6306 (2008)
11. W.M. Xia, Z. Xu, F. Wen, Z.C. Zhang, Ceram. Int. **38**, 1071–1075 (2012)
12. X.L. Dou, X.L. Liu, Y. Zhang, H. Feng, J.F. Chen, S. Du, Appl. Phys. Lett. **95**, 132904 (2009)
13. E.Q. Huang, J. Zhao, J.W. Zha, L. Zhang, R.J. Liao, Z.M. Dang, J. Appl. Phys. **115**, 194102 (2014)
14. H.W. Lu, L.Z. Liu, J.Q. Lin, W.L. Yang, L. Weng, X.R. Zhang, G.R. Chen, W. Huang, J. Appl. Polym. Sci. **134**, 45362 (2017)
15. S.H. Wang, Y. Wan, B. Sun, L.Z. Liu, W.J. Xu, Nanoscale Res Lett **9**, 522 (2014)
16. B. Zhao, M. Hamidinejad, C.X. Zhao, R.S. Li, S. Wang, Y. Kazemi, C.B. Park, J. Mater. Chem. A **7**, 133–140 (2019)
17. X.M. He, Y.M. Chen, K. Zhu, S.X. Wang, H.W. Zhang, W. He, F. Xia, X.F. Jin, Y.S. Hu, X.H. Su, Polym. Compos. **39**, E1920–E1927 (2018)
18. A. Eshraghian, M. Kamkar, M. Asgari, M. Arjmand, U. Sundararaj, Polym. Compos. **42**, 1034–1048 (2021)
19. W. Chueangchayaphan, P. Luangchuang, N. Chueangchayaphan, M.A. Sulaiman, Y. Nakaramontri, Chin. J. Polym. Sci. **39**, 725–735 (2021)
20. P. Wang, L. Yang, S. Gao, X.L. Chen, T. Cao, C. Wang, H. Liu, X.H. Hu, X.S. Wu, S.J. Feng, Advanced Composites and Hybrid Materials **4**, 639–646 (2021)
21. J.Y. Liang, Y.Z. Gu, Z.C. Zhang, S.K. Wang, M. Li, Z.G. Zhang, Nanotechnology **29**, 035701 (2017)
22. K. Silakaew, P. Thongbai, RSC Adv. **9**, 23498–23507 (2019)

23. Q.H. Deng, B.H. Chen, M.L. Bo, Y.F. Feng, Y.H. Huang, J.Q. Zhou, *Journal of Materials Chemistry C* **9**, 1051–1061 (2021)
24. X.Y. Huang, P.K. Jiang, *Adv Mater* **27**, 546–554 (2015)
25. J.M. Zhu, X.Y. Ji, M. Yin, S.Y. Guo, J.B. Shen, *Compos. Sci. Technol.* **144**, 79–88 (2017)
26. X.W. Cao, W.J. Zhao, X.J. Gong, D.L. Zhang, Q.J. Su, J.W. Zha, X.M. Yin, W. Wu, R.K.Y. Li, *Compos. A Appl. Sci. Manuf.* **148**, 106486 (2021)
27. M.J. Feng, C.H. Zhang, G.T. Zhou, T.D. Zhang, Y. Feng, Q.G. Chi, Q.Q. Lei, *IEEE Access* **8**, 81542–81550 (2020)
28. L.Z. Guan, L. Weng, X.R. Zhang, Z.J. Wu, Q. Li, L.Z. Liu, *J. Mater. Sci.* **55**, 15238–15251 (2020)
29. Y. Xuan, G.C. Jiang, Y.Y. Li, J.S. Wang, H.N. Geng, *Colloids Surf., A* **422**, 50–60 (2013)
30. L.Z. Guan, L. Weng, Q. Li, X.R. Zhang, Z.J. Wu, Y.Y. Ma, *Mater. Des.* **197**, 109241 (2021)

**Publisher's Note** Springer Nature remains neutral with regard to jurisdictional claims in published maps and institutional affiliations.